Synthesis and Analysis of Time-optimal Current Trajectory Based on Final-state Control for IPMSM

Takayuki Miyajima, Hiroshi Fujimoto
The University of Tokyo
Kashiwa, Chiba, Japan
miya@fujilab.k.u-tokyo.ac.jp, fujimoto@k.u-tokyo.ac.jp

Masami Fujitsuna
DENSO CORPORATION
Kariya, Aichi, Japan
MASAMI_FUJITSUNA@denso.co.jp

***Abstract*— This paper investigates time-optimal current trajectory of an interior permanent magnet synchronous motor (IPMSM) and achievable performance limitations. The analysis with linearized IPMSM model shows that time-optimal trajectory under voltage limit has q-axis current undershoot, d-axis current overshoot, and torque overshoot/undershoot. These achievable performance limitations are verified with final-state control which desribes current response under the voltage limit with linear matrix inequalities.**

I. INTRODUCTION

Interior permanent magnet synchronous motors (IPMSMs) are widely used for industrial applications owing to high efficiency and high power density. In order to reduce the size and improve the efficiency of IPMSM, high speed operation is desirable. However, quick torque response is difficult in high-speed region because the inverter output voltage is limited. Therefore, a quick torque control method under the voltage limit is required.

Many feedback control methods had been proposed. Modulation index feedback control methods [1], [2] modify d-axis current reference with feedback controller so that torque tracks reference under voltage limit. Voltage phase control methods [3], [4] control the torque by the voltage phase only under the voltage limit. In order to achieve quick torque control, a feedforward control method is essential. Model predictive control [5], [6] can consider the voltage limit easily and optimize output trajectory. [7] derives a voltage limiter which maximizes the torque response under the voltage limit by using Lagrange multiplier. In [8], current trajectory is optimized based on calculus of variations. [9] optimizes the torque response of IPMSM by using dynamic programming and Pontryagin's maximum principle. However, in past researches, achievable performance limitations of torque trajectory and current trajectory under voltage limit are not analyzed precisely.

The authors proposed feedforward current control in flux-weakening region for a surface permanent magnet synchronous motor based on final-state control [10]. This control method describes current response with linear matrix inequalities (LMIs) [11] and derives time-optimal current trajectory by solving these LMIs. Moreover, the authors analyzed the derived current trajectory using the voltage limit circle with transient term and showed that q-axis current undershoot and d-axis current overshoot are essential for quick response. However, this method cannot analyze torque response of IPMSM.

On the other hand, the authors proposed a model-based design method of the voltage phase controller using a linearized transfer function from the voltage phase to the torque [12]. Utilizing this linearized transfer function, torque trajectory can be analyzed.

This paper analyzes achievable performance limitations of current trajectory and torque trajectory with zeros of linearized transfer functions. This analysis shows that time-optimal trajectory cannot avoid d-axis current overshoot, q-axis current undershoot and torque undershoot/overshoot. Moreover, in this paper, time-optimal current trajectory and quasi time-optimal torque trajectory are derived based on final-state control. Simulation results and experimental results of these trajectories verify analyzed achievable performance limitations.

II. MODEL AND DISCRETIZATION

The voltage equation of IPMSM in dq-axis is given by

$$\dot{\boldsymbol{x}}(t) = \boldsymbol{A}_c(\omega_e)\boldsymbol{x}(t) + \boldsymbol{B}_c\left(\boldsymbol{v}(t) + \boldsymbol{v}_{emf}(\omega_e)\right), \tag{1}$$

$$\boldsymbol{y}(t) = \boldsymbol{C}_c\boldsymbol{x}(t), \tag{2}$$

$$\left[\begin{array}{c|c} \boldsymbol{A}_c(\omega_e) & \boldsymbol{B}_c \\ \hline \boldsymbol{C}_c & \boldsymbol{0} \end{array}\right] := \left[\begin{array}{cc|cc} -\frac{R}{L_d} & \omega_e\frac{L_q}{L_d} & \frac{1}{L_d} & 0 \\ -\omega_e\frac{L_d}{L_q} & -\frac{R}{L_q} & 0 & \frac{1}{L_q} \\ \hline \multicolumn{2}{c|}{\boldsymbol{I}} & \multicolumn{2}{c}{\boldsymbol{0}} \end{array}\right]$$

$$\boldsymbol{x} = [i_d\ i_q]^T,\ \boldsymbol{v} = [v_d\ v_q]^T,\ \boldsymbol{v}_{emf}(\omega_e) := [0\ \ -\omega_e K_e]^T,$$

$$v_d := -V_a\sin\delta,\ \ v_q := V_a\cos\delta$$

where v_d, v_q, i_d, i_q, L_d, and L_q are the d- and q-axis voltages, currents, and inductances, R is the stator winding resistance, ω_e is the electric angular velocity, K_e is the back EMF constant, V_a is the voltage amplitude, and δ is the voltage phase. The torque T_e is represented by

$$T_e = K_{mt}i_q + K_{rt}i_d i_q. \tag{3}$$

where $K_{mt} := PK_e$, $K_{rt} := P(L_d - L_q)$, and P is the number of pole pairs.

In order to discretize a plant, a zero-order hold is generally applied. However, in the case of single-phase inverter, it cannot output arbitrary voltage. Therefore, in order to control instantaneous values precisely, the zero-order hold is not suitable. When the pulse is allocated in the center of the control period

T_u, a precise discrete time plant model in which the input is ON time of the pulse can be given by discretizing based on PWM hold [14].

(1) is discretized based on PWM hold. Here, it is assumed that the speed variation during one control period can be neglected. Hence, the back EMF $\omega_e K_e$ can be presumed as the zero-order hold. The PWM hold model of IPMSM is given as

$$\begin{aligned}\boldsymbol{x}[k+1] &= \boldsymbol{A}_s(\omega_e)\boldsymbol{x}[k] + \boldsymbol{B}_s(\omega_e)\Delta\boldsymbol{T}[k] \\ &\quad + \boldsymbol{B}_{s2}(\omega_e)\boldsymbol{v}_{emf}(\omega_e), \quad (4)\\ \boldsymbol{y}[k] &= \boldsymbol{C}_s\boldsymbol{x}[k], \quad (5)\\ \boldsymbol{A}_s(\omega_e) &:= e^{\boldsymbol{A}_c(\omega_e)T_u},\ \boldsymbol{B}_s(\omega_e) := e^{\boldsymbol{A}_c(\omega_e)\frac{T_u}{2}}\boldsymbol{B}_c V_{dc},\\ \boldsymbol{B}_{s2}(\omega_e) &:= \boldsymbol{A}_c^{-1}(\omega_e)\left(e^{\boldsymbol{A}_c(\omega_e)T_u} - \boldsymbol{I}\right)\boldsymbol{B}_c,\ \boldsymbol{C}_s := \boldsymbol{C}_c,\end{aligned}$$

where V_{dc} is the dc-bus voltage of a three-phase inverter, $\Delta\boldsymbol{T} = [\Delta T_d \quad \Delta T_q]^T$, and ΔT_d, ΔT_q are the d-axis and q-axis ON time.

III. Analysis with linearized model

Under the voltage limit, the control input is voltage phase only but the relationship between currents and voltage phase is nonlinear. Therefore, in order to analyze current response under the voltage limit, the voltage equation of IPMSM is linearized.

The linearized model of IPMSM in which the inputs are the voltage phase δ and the voltage amplitude V_a is expressed as follows: [12]

$$\begin{bmatrix}\Delta i_d\\ \Delta i_q\end{bmatrix} = \begin{bmatrix}\Delta P_{11}(s) & \Delta P_{12}(s)\\ \Delta P_{21}(s) & \Delta P_{22}(s)\end{bmatrix}\begin{bmatrix}\Delta V_a\\ \Delta\delta\end{bmatrix}, \quad (6)$$

$$\Delta P_{11}(s) := \frac{-\frac{1}{L_d}\sin\delta_o\left\{s + \frac{R}{L_q} - \omega_e\tan\left(\frac{\pi}{2} - \delta_o\right)\right\}}{s^2 + \left(\frac{R}{L_d} + \frac{R}{L_q}\right)s + \frac{R^2}{L_d L_q} + \omega_e^2},$$

$$\Delta P_{12}(s) := \frac{-\frac{V_{ao}}{L_d}\cos\delta_o\left(s + \frac{R}{L_q} + \omega_e\tan\delta_o\right)}{s^2 + \left(\frac{R}{L_d} + \frac{R}{L_q}\right)s + \frac{R^2}{L_d L_q} + \omega_e^2},$$

$$\Delta P_{21}(s) := \frac{\frac{1}{L_q}\cos\delta_o\left(s + \frac{R}{L_d} + \omega_e\tan\delta_o\right)}{s^2 + \left(\frac{R}{L_d} + \frac{R}{L_q}\right)s + \frac{R^2}{L_d L_q} + \omega_e^2},$$

$$\Delta P_{22}(s) := \frac{-\frac{V_{ao}}{L_d}\sin\delta_o\left\{s + \frac{R}{L_q} - \omega_e\tan\left(\frac{\pi}{2} - \delta_o\right)\right\}}{s^2 + \left(\frac{R}{L_d} + \frac{R}{L_q}\right)s + \frac{R^2}{L_d L_q} + \omega_e^2},$$

$$\Delta i_d := i_d - i_{do},\ \Delta i_q := i_q - i_{qo},$$
$$\Delta V_a := V_a - V_{ao}, \Delta\delta := \delta - \delta_o,$$

where V_{ao}, δ_o, i_{do}, and i_{qo} are the voltage amplitude, the voltage phase, the d-axis current, and the q-axis current on the equilibrium point ($\dot{\boldsymbol{x}} = 0$).

The zeros of $\Delta P_{12}(s)$ and $\Delta P_{22}(s)$ are represented by (7) and (8), respectively.

$$z_{12} = -\frac{R}{L_q} - \omega_e\tan\delta_o. \quad (7)$$

$$z_{22} = -\frac{R}{L_d} + \omega_e\tan\left(\frac{\pi}{2} - \delta_o\right). \quad (8)$$

The voltage phase control operates within monotone increasing range between torque and voltage phase. If the stator winding resistance R can be neglected, the average torque $\bar{T}_e$ is represented by

$$\bar{T}_e = \frac{K_{mt}V_a}{\omega_e L_d}\sin\delta + \frac{V_a^2}{2\omega_e^2}\left(\frac{1}{L_q} - \frac{1}{L_d}\right)\sin 2\delta. \quad (9)$$

From this equation, the monotone increasing range is $[-\pi/2$ $\pi/2]$. In the flux-weakening region, $\frac{R}{L_d} \ll \omega_e$ and $\frac{R}{L_q} \ll \omega_e$. Therefore, during motoring mode ($0 < \delta_o < \pi/2$), $\Delta P_{12}(s)$ and $\Delta P_{22}(s)$ have a stable zero and an unstable zero, respectively. This means that current trajectory under voltage limit has two achievable performance limitation: trade-offs between d-axis current overshoot and settling time and between q-axis current overshoot and settling time. In particular, $\Delta P_{12}(s)$ has a slow stable zero in low-speed and low-torque region and time-optimal current trajectory has large d-axis current overshoot under the voltage limit. On the other hand, in flux-weakening region and high-torque region, $\Delta P_{22}(s)$ has a slow unstable zero. Therefore, time-optimal current trajectory cannot avoid large q-axis current undershoot.

Similarly, torque response under the voltage limit is analyzed. The torque can be linearized as

$$T_e \simeq T_{eo} + (K_{mt} + K_{rt}i_{do})\Delta i_q + K_{rt}i_{qo}\Delta i_d, \quad (10)$$

where T_{eo} is the torque at equilibrium point. From (6) and (10), the linearized transfer function from the voltage phase to the torque is experessed by

$$\Delta P_{T2}(s) = \frac{\Delta T_e}{\Delta\delta} = \frac{b_{T21}s + b_{T20}}{s^2 + \left(\frac{R}{L_d} + \frac{R}{L_q}\right)s + \frac{R^2}{L_d L_q} + \omega_e^2},$$

$$b_{T21} := -V_{ao}\sqrt{\frac{K_1^2}{L_q^2} + \frac{K_2^2}{L_d^2}}\sin\left(\delta_o + \tan^{-1}\frac{K_2 L_q}{K_1 L_d}\right),$$

$$b_{T20} := -V_{ao}\frac{R}{L_d L_q}\sqrt{K_1^2 + K_2^2}\sin\left(\delta_o + \tan^{-1}\frac{K_2}{K_1}\right) + V_{ao}\omega_e\sqrt{\frac{K_1^2}{L_q^2} + \frac{K_2^2}{L_d^2}}\cos\left(\delta_o + \tan^{-1}\frac{K_2 L_q}{K_1 L_d}\right),$$

$$K_1 := K_{mt} + K_{rt}i_{do},\ K_2 := K_{rt}i_{qo}.$$

A zero of $\Delta P_{T2}(s)$ is expressed by $z_{T2} := -b_{T20}/b_{T21}$. However, it is a complex nonlinear function of the operation point. Thus, the value of the zero is given by numerical calculation. The result is shown in Fig. 1. Here, Table I illustrates the nominal parameters of the test.

As shown in Fig. 1, the value of the zero depends on the operation point. Fig. 1 demonstrates that the plant has a slow unstable zero in high-speed and high-torque region and time-optimal torque trajectory cannot avoid large undershoot. On

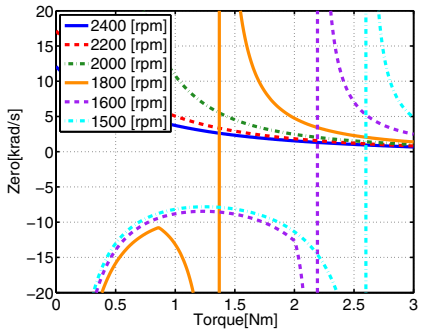

Fig. 1. A zero of linearized plant model ΔP_{T2}

TABLE I

PARAMETERS UNDER THE TEST.

d-axis inductance L_d	0.671 mH
q-axis inductance L_q	1.69 mH
Resistance R	140.2 mΩ
Pairs of poles P	3
Back EMF constant K_e	44.25 mV/(rad/s)
Inverter dc-bus voltage V_{dc}	36.0 V
Maximum modulation index $M_{\max}$	1.15

the other hand, at low-speed and low-torque region, the plant has a stable zero but it is fast. Therefore, time-optimal torque trajectory has small overshoot.

IV. CONTROL SYSTEM DESIGN

The block diagram of the control system is described as Fig. 2. This control system consists of the 2-DOF control system. Each control method uses the same feedback controller $\boldsymbol{C}_2[z]$ and the different feedforward controller $\boldsymbol{C}_1[z]$.

The current reference generator makes the d-axis and the q-axis references which are a intersection point of constant torque curve with MTPA curve or voltage limit ellipse.

All control input limiters are described by

$$\Delta\tilde{\boldsymbol{T}}[k] = \begin{cases} \dfrac{\Delta\boldsymbol{T}[k]}{|\Delta\boldsymbol{T}[k]|}\Delta T_{\max} & \text{if } |\Delta\boldsymbol{T}[k]| > \Delta T_{\max} \\ \Delta\boldsymbol{T}[k] & \text{otherwise} \end{cases}, \quad (11)$$

where $\Delta T_{\max}$ is the maximum value of dq-axis ON time vector amplitude and $\Delta\tilde{\boldsymbol{T}}[k]$ is the limiter output.

$\Delta\theta_e(:= 0.5\omega_e T_u)$ in the space vector modulation (SVM) is the sampling error compensation for the dq/2-phase transform [15]. Here, T_u is the control period.

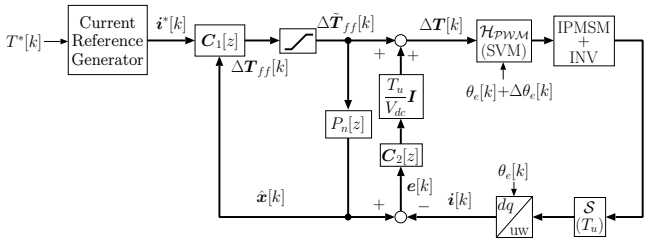

Fig. 2. Control System

The FB controller $\boldsymbol{C}_2[z]$ is represented as

$$\boldsymbol{C}_2[z] = \begin{bmatrix} C_d[z] & 0 \\ 0 & C_q[z] \end{bmatrix}, \quad (12)$$

where $C_d[z]$ and $C_q[z]$ are the d-axis and q-axis current FB controllers. These controllers are designed without taking decoupling term in consideration. Therefore, the plant models of d-axis and q-axis current FB controller designs are obtained as

$$\frac{i_d^*}{v_d} = \frac{1}{L_d s + R}, \quad \frac{i_q^*}{v_q} = \frac{1}{L_q s + R}, \quad (13)$$

respectively. $C_d(s)$ and $C_q(s)$ are designed with the coefficient diagram method [16]. By discretizing $C_d(s)$ and $C_q(s)$ by Tustin transform with the control period T_u, $C_d[z]$ and $C_q[z]$ are given. Here, if $|\Delta\boldsymbol{T}[k]| > \Delta T_{\max}$, anti-windup control is applied to $C_d[z]$ and $C_q[z]$ [17].

A. Method 1 (Simple inverse system)

The inverse system of the PWM hold model is obtained as

$$\Delta\boldsymbol{T}_{ff}[k] = -\boldsymbol{B}_s^{-1}(\omega_e)\boldsymbol{A}_s(\omega_e)\boldsymbol{x}_0[k] + \boldsymbol{B}_s^{-1}(\omega_e)\boldsymbol{i}^*[k] - \boldsymbol{B}_s^{-1}(\omega_e)\boldsymbol{B}_{s2}(\omega_e)\boldsymbol{u}_{emf}(\omega_e). \quad (14)$$

From this stable inverse system, the FF controller $\boldsymbol{C}_1[z]$ is designed. Therefore, if the plant is nominal and the control input is not limited, $\boldsymbol{C}_1[z]$ assures the perfect tracking at the sample time. Here, $\boldsymbol{x}_0[k] := [i_{d0}[k] \;\; i_{q0}[k]]^T$ in Fig. 2 is the nominal output which takes the input limit in consideration. If the control input is limited, $\hat{\boldsymbol{x}}[k]$ is not the same with the current reference delayed one sample $\boldsymbol{i}^*[k-1]$.

B. Method 2 (Optimal current trajectory) [10]

The final-state control transits an initial state to a final state by prescribed time interval [13]. Here, the final-state control considering the voltage limit is expressed as a programming problem whose evaluation function and constraint functions are quadratic function and quadratic inequality in the form of LMI. The FF controller $\boldsymbol{C}_1[z]$ generates FF input by solving these LMIs.

From PWM hold model of IPMSM, the final state $\boldsymbol{x}[N]$ is represented with the initial state $\boldsymbol{x}[0]$ as follows:

$$\boldsymbol{Y} = \boldsymbol{\Sigma}\boldsymbol{U} \quad (15)$$

$$\boldsymbol{Y} := \boldsymbol{x}[N] - \boldsymbol{A}_s^N\boldsymbol{x}[0] - \boldsymbol{\Sigma}_2\boldsymbol{U}_{emf} \quad (16)$$

$$\boldsymbol{\Sigma} := \begin{bmatrix} \boldsymbol{A}_s^{N-1}\boldsymbol{B}_s & \boldsymbol{A}_s^{N-2}\boldsymbol{B}_s & \cdots & \boldsymbol{B}_s \end{bmatrix} \quad (17)$$

$$\boldsymbol{\Sigma}_2 := \begin{bmatrix} \boldsymbol{A}_s^{N-1}\boldsymbol{B}_{s2} & \boldsymbol{A}_s^{N-2}\boldsymbol{B}_{s2} & \cdots & \boldsymbol{B}_{s2} \end{bmatrix} \quad (18)$$

$$\boldsymbol{U} := \begin{bmatrix} \Delta\boldsymbol{T}^T[0] \; \Delta\boldsymbol{T}^T[1] \cdots \Delta\boldsymbol{T}^T[N-1] \end{bmatrix}^T \quad (19)$$

$$\boldsymbol{U}_{emf} := \begin{bmatrix} \boldsymbol{v}_{emf}^T & \boldsymbol{v}_{emf}^T & \cdots & \boldsymbol{v}_{emf}^T & \boldsymbol{v}_{emf}^T \end{bmatrix}^T \quad (20)$$

Here, it is assumed that ω_e is constant in this derivation.

The FF input series $\boldsymbol{U}$ which satisfies (15) is not determined uniquely. Thereupon, the square sum of the current error is

minimized. The cost function J is represented by

$$J = \boldsymbol{E}^T \boldsymbol{Q} \boldsymbol{E}, \quad \boldsymbol{Q} > \boldsymbol{0}, \tag{21}$$

$$\boldsymbol{E} := \boldsymbol{I}^* - \boldsymbol{A}\boldsymbol{x}[0] - \boldsymbol{B}\boldsymbol{U} - \boldsymbol{B}_2 \boldsymbol{U}_{emf}, \tag{22}$$

$$\boldsymbol{A} := \begin{bmatrix} \boldsymbol{A}_s & \boldsymbol{A}_s^2 & \cdots \boldsymbol{A}_s^N \end{bmatrix}^T, \tag{23}$$

$$\boldsymbol{B} := \begin{bmatrix} \boldsymbol{B}_s & 0 & \cdots & 0 \\ \boldsymbol{A}_s \boldsymbol{B}_s & \boldsymbol{B}_s & \cdots & 0 \\ \vdots & \vdots & \ddots & \vdots \\ \boldsymbol{A}_s^{N-1} \boldsymbol{B}_s & \boldsymbol{A}_d^{N-2} \boldsymbol{B}_s & \cdots & \boldsymbol{B}_s \end{bmatrix}, \tag{24}$$

$$\boldsymbol{B}_2 := \begin{bmatrix} \boldsymbol{B}_{s2} & 0 & \cdots & 0 \\ \boldsymbol{A}_s \boldsymbol{B}_{s2} & \boldsymbol{B}_{s2} & \cdots & 0 \\ \vdots & \vdots & \ddots & \vdots \\ \boldsymbol{A}_s^{N-1} \boldsymbol{B}_{s2} & \boldsymbol{A}_s^{N-2} \boldsymbol{B}_{s2} & \cdots & \boldsymbol{B}_{s2} \end{bmatrix}, \tag{25}$$

$$\boldsymbol{I}^* := \begin{bmatrix} (\boldsymbol{i}^*)^T & (\boldsymbol{i}^*)^T \cdots (\boldsymbol{i}^*)^T \end{bmatrix}^T. \tag{26}$$

Moreover, (4) is controllable. Thus, $\boldsymbol{\Sigma}$ is full row rank. There, $\boldsymbol{\Sigma}^\perp \in \mathbb{R}^{2N \times (2N-2)}$ and $\boldsymbol{\Sigma}^\dagger \in \mathbb{R}^{2N \times 2}$ which fulfill $\boldsymbol{\Sigma}\boldsymbol{\Sigma}^\perp = \boldsymbol{0}$ and $\boldsymbol{\Sigma}\boldsymbol{\Sigma}^\dagger = \boldsymbol{I}$ respectively are defined. $\boldsymbol{U}$ is described by

$$\boldsymbol{U} := [\boldsymbol{\Sigma}^\dagger \quad \boldsymbol{\Sigma}^\perp] \tilde{\boldsymbol{U}}, \quad \tilde{\boldsymbol{U}} = \begin{bmatrix} \boldsymbol{Y} & \boldsymbol{q} \end{bmatrix}^T, \tag{27}$$

where $\boldsymbol{q} \in \mathbb{R}^{(2N-2)\times 1}$ is a free parameter.

By substituting (22) and (27) to (21), the cost function J is transformed as follows:

$$J = R(\boldsymbol{q}) + \boldsymbol{S}^T(\boldsymbol{q}) \boldsymbol{Q} \boldsymbol{S}(\boldsymbol{q}), \tag{28}$$

$$\boldsymbol{Z} := \boldsymbol{I}^* - \boldsymbol{A}\boldsymbol{x}[0] - \boldsymbol{B}\boldsymbol{\Sigma}^\dagger \boldsymbol{Y} - \boldsymbol{B}_2 \boldsymbol{U}_{emf}, \tag{29}$$

$$R(\boldsymbol{q}) := \boldsymbol{Z}^T \boldsymbol{Q} \boldsymbol{Z} - 2\boldsymbol{Z}^T \boldsymbol{Q} \boldsymbol{S}(\boldsymbol{q}), \tag{30}$$

$$\boldsymbol{S}(\boldsymbol{q}) := \boldsymbol{B}\boldsymbol{\Sigma}^\perp \boldsymbol{q}. \tag{31}$$

With LMI, the condition which satisfies $J < \gamma$ for provided γ is given by (32) [18].

$$\begin{bmatrix} \gamma - R(\boldsymbol{q}) & \boldsymbol{S}(\boldsymbol{q})^T \\ \boldsymbol{S}(\boldsymbol{q}) & \boldsymbol{Q}^{-1} \end{bmatrix} > 0. \tag{32}$$

Next, the voltage limit is described with LMI. The voltage limits at each sampling point are described as

$$\Delta \boldsymbol{T}^T[k] \Delta \boldsymbol{T}[k] \le \Delta T_{\max}^2 \ \ (k = 0, 1, \cdots, N-1). \tag{33}$$

Here, $\boldsymbol{g}(i) \in \mathbb{R}^{2\times 2N}$ $(i := 2k+1)$ of which (1, i) th and (2, $i+1$) th entries are 1 and other entries are 0 is defined. $\boldsymbol{g}(i)$ separates input vector $\Delta \boldsymbol{T}[k]$ as follows:

$$\Delta \boldsymbol{T}[k] = \boldsymbol{g}(i) \boldsymbol{U}(\boldsymbol{q}). \tag{34}$$

From (34), (33) is expressed as LMI

$$\begin{bmatrix} \Delta T_{\max}^2 & \boldsymbol{U}(\boldsymbol{q})^T \boldsymbol{g}(i)^T \\ \boldsymbol{g}(i) \boldsymbol{U}(\boldsymbol{q}) & \boldsymbol{I} \end{bmatrix} \ge 0, \tag{35}$$

where $i = 2k+1$, $k = 0, 1, \cdots, N-1$.

By minimizing γ under (32) and (35), the FF input is obtained. If the mininum prescribed time interval under (32) and (35) is selected, the derived trajecotry is time-optimal.

C. Method 3 (Quasi-optimal torque trajectory)

It is desired that torque trajectory has no overshoot and no undershoot. However, the analysis in section III shows that time-optimal trajectory has an undershoot or an overshoot. Therefore, the torque should be constrained.

(3) can be expressed as follows:

$$T_e = K_{mt} i_q + \begin{bmatrix} i_d \\ i_q \end{bmatrix}^T \begin{bmatrix} 0 & \frac{K_{rt}}{2} \\ \frac{K_{rt}}{2} & 0 \end{bmatrix} \begin{bmatrix} i_d \\ i_q \end{bmatrix}. \tag{36}$$

The coefficient matrix is not positive definite. Thus, the torque of IPMSM cannot be represented with LMI though the linearized torque which is described as (10) can be expressed by LMI. An overshoot and an undershoot happen around the final-state and the initial state, respectively. Therefore, an overshoot and an undershoot can be suppressed by LMIs which constrain linearized torques around the final state and the initial state with little modeling error.

With the linearized torque around an initial state, the constraint function for a torque undershoot is represented by

$$\begin{aligned} &\mathrm{sgn}(T_e^* - T_e[0]) \{(K_{mt} + K_{rt} i_d[0]) i_q(\boldsymbol{q})[k] \\ &+ K_{rt} i_q[0] i_d(\boldsymbol{q})[k] - K_{rt} i_d[0] i_q[0] - T_e[0]\} \ge 0. \end{aligned} \tag{37}$$

Similarly, by using the linearized torque around the final state, the constraint function for a torque overshoot is described by

$$\begin{aligned} &\mathrm{sgn}(T_e^* - T_e[0]) \{T_e^* - (K_{mt} + K_{rt} i_d^*) i_q(\boldsymbol{q})[k] \\ &- K_{rt} i_q^* i_d(\boldsymbol{q})[k] + K_{rt} i_d^* i_q^*\} \ge 0. \end{aligned} \tag{38}$$

By minimizing γ under (32), (35), (37), and (38), the FF inputs for quasi-optimal torque trajectory can be derived.

V. Simulation

The achievable performance limitations are discussed with simulation results. The parameters of simulations are the same as explained in section III. In order to suppress model error, d-axis and q-axis references are selected from torque reference as the voltage amplitude on steady-state is within $0.95 V_{a\max}$ ($V_{a\max} := \sqrt{\frac{3}{2}} \frac{V_{dc}}{2} M_{\max}$). The control period T_u is 0.1 ms.

Simulation results of method 1, method 2, and method 3 at 2000 rpm are reported as Fig. 3, 4, and 5, respectively. In method 2 and method 3, the prescribed time interval N is chosen to be minimum (Method 2: N=27, Method 3: N = 30). Therefore, the derived trajectories are time-optimal. The dotted lines in Fig. 3(d), 4(d), and 5(d) describes the maximum modulation index $M_{\max}$. T_0 is the nominal torque which is calculated with the nominal output $\boldsymbol{x}_0$.

From the analysis in section III, at 2000 rpm, $\Delta P_{12}(s)$, $\Delta P_{22}(s)$, and $\Delta P_{T2}(s)$ have a stable zero, an unstable zero, and an unstable zero, respectively. Method 1 causes a little q-axis current undershoot and a little torque undershoot. However, it does not cause d-axis current overshoot. Therefore, it cannot achieve quick response due to the trade-off between d-axis current overshoot and settling time. On the other hand, method 2 succeeds in minimizing the settling time. It makes the large d-axis current overshoot, the large q-axis current

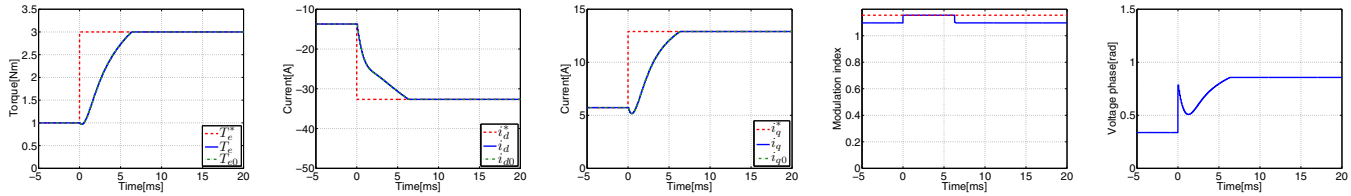

(a) Torque (b) i_d (c) i_q (d) Modulation index (e) δ

Fig. 3. Simulation results (Method 1).

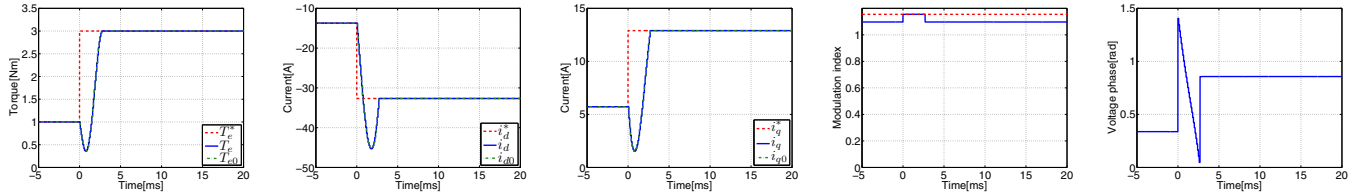

(a) Torque (b) i_d (c) i_q (d) Modulation index (e) δ

Fig. 4. Simulation results (Method 2, N=27).

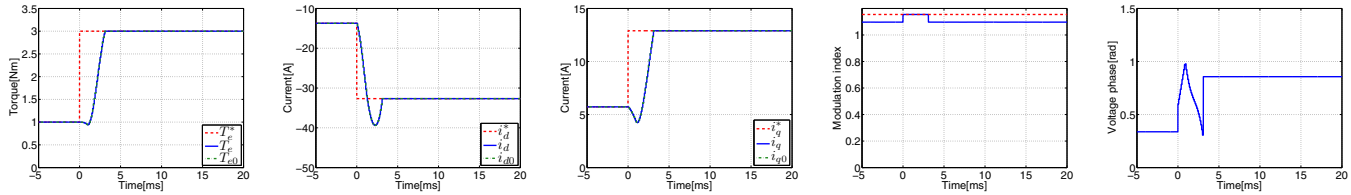

(a) Torque (b) i_d (c) i_q (d) Modulation index (e) δ

Fig. 5. Simulation results (Method 3, N=30).

undershoot, and the large torque undershoot. Method 3 suppresses the torque undershoot but the little torque undershoot happens due to linearized error. Compared with method 2, the d-axis current overshoot and the q-axis current undershoot decrease and the settling time increases. These simulation results correspond with the analysis in section II and it is confirmed that current response and torque response under the voltage limit have achievable performance limitations.

VI. Experiment

Experiments were performed in the same condition as simulations. In method 2 and method 3, FF inputs cannot be derived during one sampling period (0.1 ms). Therefore, FF inputs which are the same with simulations were calculated by off-line. If the nonimal output does not reach the final state during the prescribed time interval due to speed variation, FF inputs are generated in the same way as method 1.

Fig. 6, 7, and 8 describe experimental results of method 1, method 2, and method 3 at 2000 rpm, respectively. Tracking errors between the plant outputs and the nominal outputs happen due to the modeling error though all experimental results are exactly similar to simulation results. The current trajectory of Method 1 has no d-axis current overshoot and a little q-axis current undershoot. Therefore, the settling time is the longest due to the trade-offs. Method 3 shortens the settling time with the little torque undershoot because the d-axis current overshoot is happened. Method 2 achieves the shortest settling time. It makes the large d-axis current overshoot, the large q-axis current undershoot, and the large torque undershoot.

As with simulation results, experimental results show achievable performance limitations of the current trajectory and the torque trajectory.

VII. Conclusion

This paper analyzes the achievable performance limitations of the current and the torque by using zeros of linearized plant models. The analysis shows that the time-optimal trajectory under the voltage limit cannot avoid a q-axis current undershoot, a d-axis current overshoot, and a torque overshoot or a torque undershoot.

The time-optimal current trajectory and the quasi-optimal torque trajectory are synthesized based on the final-state control. Simulation results and experimental results verify the achievable performance limitations of the time-optimal trajectory. The quasi-optimal torque trajectory which suppresses the torque undershoot under the voltage limit lengthens the settling time because the transfer function between torque and voltage phase has an unstable zero. Real-time calculation of the proposed methods is difficult. However, the proposed methods reperesent current response under the voltage limit with LMI. Therefore, optimal current response under the voltage limit can be calcurlated easily with an inter-point method.

In future work, the constraint condition of the torque is considered more precisely and the time-optimal torque trajectory is derived.

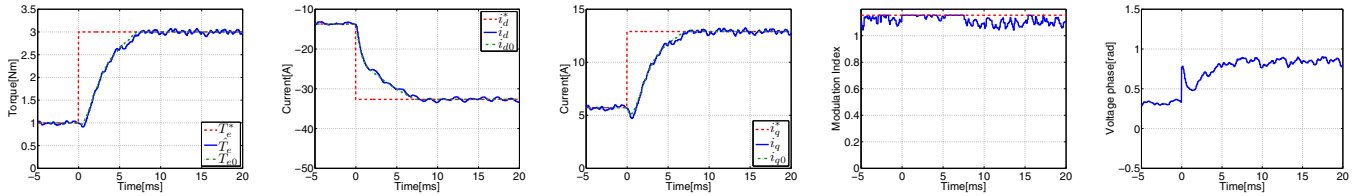

(a) Torque (b) i_d (c) i_q (d) Modulation index (e) δ

Fig. 6. Experimantal results (Method 1).

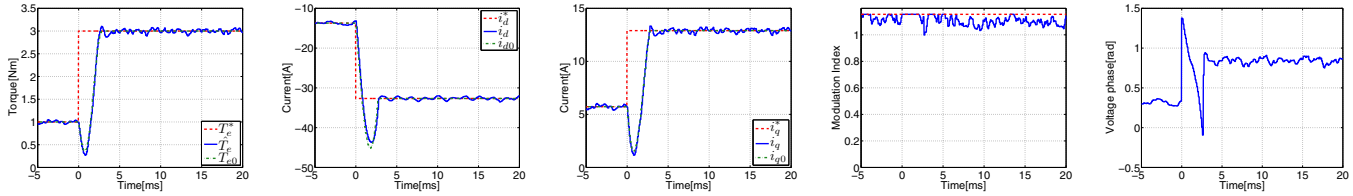

(a) Torque (b) i_d (c) i_q (d) Modulation index (e) δ

Fig. 7. Experimantal results (Method 2, N=27).

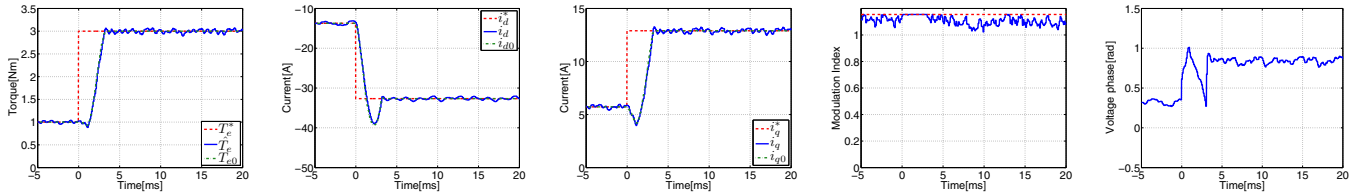

(a) Torque (b) i_d (c) i_q (d) Modulation index (e) δ

Fig. 8. Experimantal results (Method 3, N=30).

REFERENCES

[1] K. Kondo, K. Matsuoka, Y. Nakazawa, and H. Shimizu: "Torque feedback control for salient pole permanent magnet synchronous motor at weakening flux control range", T.IEEJapan, Vol.119-D, No.10, pp.1155–1164, 1999 (in Japanese).

[2] T.-S. Kwon, G.-Y. Choi, M.-S. Kwak, and S.-K. Sul : "Novel Flux-Weakening Control of an IPMSM for Quasi-Six-Step Operation", IEEE Trans. Ind. Appl., Vol.44, NO.6, pp.1722–1723, 2008.

[3] H. Nakai, H. Ohtani, E. Satoh, and Y. Inaguma: "Development and Testing of the Torque Control for the Permanent-Magnet Synchronous Motor", IEEE Trans. Ind. Electron., Vol.52, No.3, pp.800–806, 2005.

[4] W. Hatsuse, Y. Notohara, K. Ohi, K. Tobari, K. Tamura, C. Unoko, and Y. Iwaji: "A Stable Field-Weakening Control Using Voltage Phase Operations in the High-Power Region", The 2010 International Power Electronics Conference, pp.599–604, 2010.

[5] T. Geyer: "Computationally Efficient Model Predictive Direct Torque Control", IEEE Trans. Power Electronics, Vol. 26, No. 10, pp. 2804–2816, 2011.

[6] T. Maeda and S. Doki: "Improvement of Torque Control System of PMSM based on Model Predictive Control", The 37th Annual Conference on IEEE Industrial Electronics Society, pp. 1891–1896, 2011.

[7] S. Lerdudomsak, S. Doki, and S. Okuma: "Novel Techniques for Fasr Torque Response of IPMSM Based on Space-Vector Control Method in Voltage Saturation Range", The 33rd Annual Conference of the IEEE Industrial Electronics Society, pp. 1015–1020, 2007.

[8] N. Bianchi, S. Bolognani, and M. Zigliotto: "Time optimal current control for PMSM drives", The 28th Annual Conference of the IEEE Industrial Electronics Society, pp.745–750, 2002.

[9] J. S. Lee, R. D. Lorenz, and M. A. Valenzuela: "Time Optimal and Loss Minimizing Deadbeat-Direct Torque and Flux Control for Interior Permanent Magnet Synchronous Machines", The 2012 IEEE Energy Conversion Congress and Exposition, pp.2568–2575, 2012.

[10] T. Miyajima, H. Fujimoto, and M. Fujitsuna: "Feedforward control for SPMSM with Final State Control Based on Voltage Limit Circle with Transient Term", The 2011 IEEE Energy Conversion Congress and Exposition, pp.3913–3919, 2011.

[11] S. Boyd, L. E. Ghaoui, E. Feron, and V. Balakrishnan: "Linear Matrix Inequalities in System and Control Theory", Society for Industrial and Applied Mathematics, 1994.

[12] T. Miyajima, H. Fujimoto, and M. Fujitsuna: "Model-Based Design of Voltage Phase Controller for SPMSM in Field-Weakening Region", The 28th Annual IEEE Applied Power Electronics Conference and Exposition, 2013 (to be presented).

[13] T. Totani and H. Nishimura: "Final-State Control Using Compensation Input", Trans. of the SICE, Vol.30, No.3, pp.253–260, 1994.

[14] K. P. Gokhale, A. Kawamura, and R. G. Hoft: "Deat beat microprocessor control of PWM inverter for sinusoidal output waveform synthesis", IEEE Trans. Ind. Appl., Vol. 23, No. 3, pp. 901–910 (1987).

[15] J. Kudo, T. Noguchi, M. Kawakami, and K. Sano: "Mathematical Model Errors and Their Compensations of IPM Motor Control System", IEE of Japan Technical Meeting Record, IEE Japan, SPC-08-25, pp.25–31, 2008 (in Japanese).

[16] S. Manabe: "Coefficient Diagram Method", 14th IFAC Symposium on Automatic Control in Aerospace, pp. 322-327, 1998.

[17] K. Ohishi, E. Hayasaka, T. Nagano, and H. Masaya: "High-performance speed servo system considering Voltage saturation of a vector-controlled induction motor", IEEE Trans. Ind. Electron., Vol. 5., NO. 3, pp. 795–802, 2006.

[18] M. Hirata, T. Hasegawa, and K. Nonami: "Seek Control of Hard Disk Drives Based on Final-State Control Tracking Account of the Frequency Compensates and the Magnitude of Control Input", The 7th International Workshop on Advanced Motion Control, pp.40–46, 2002.